第 48 卷 第 8 期
2021 年 8 月

湖南大学学报（自然科学版）
Journal of Hunan University（Natural Sciences）

Vol. 48. No. 8.
August 2021

Open Access Article

Performance Analysis of Induction Motor Based on Core Material

Ali Failh Challoop[1], Ahmed Jasim Sultan[1], Mehdi F. Bonneya[2]

[1] Electrical Power Engineering Department, Electrical Engineering Technical College, Middle Technical University, Baghdad, Iraq

[2] Kut Technical Institute, Middle Technical University, Wasit, Iraq

Abstract: One of the most important factors of an induction motor is to obtain the best electromagnetic torque for an induction motor, which depends on the type and specification of the magnetic materials of the stator and rotor. The proposed method in this paper is based on selecting the core materials which can have minimum core losses, minimum cogging torque, good electromagnetic torque, and best efficiency. The purpose of this research is to improve the electromagnetic torque of a three-phase induction motor by investigating core magnetic materials and analyzing the motor's performance. The five magnetic materials (Cobalt Iron, Steel 1010, Steel 1018, Silicon Steel M270, and Nickel-Iron) are used. The test method is carried out using a two-dimensional flow environment to examine the electrical and mechanical properties of magnetic materials that are used based on finite element analysis (FEA). The simulation results showed that torque, efficiency, Iron losses (Bertotti), and steady-state time of speed are 37.52 N.m, 91.1%, 84.78 w, and 0.25 sec, respectively, for nickel-iron, which was the best material compared to the performance of other materials. These materials were further tested for their performance in two cases (no load and at load).

Keywords: core magnetic materials, motor performance, induction motor, flux environment, finite element.

基于磁芯材料的感应电机性能分析

摘要：感应电机最重要的因素之一是为感应电机获得最佳电磁转矩，这取决于定子和转子磁性材料的类型和规格。本文提出的方法是基于选择具有最小磁芯损耗、最小齿槽转矩、良好电磁转矩和最佳效率的磁芯材料。本研究的目的是通过研究铁芯磁性材料和分析电机性能来提高三相感应电机的电磁转矩。使用五种磁性材料（钴铁、钢1010、钢1018、硅钢米270和镍铁）。该测试方法使用二维流动环境进行，以检查基于有限元分析(有限元分析)使用的磁性材料的电气和机械性能。模拟结果表明，镍铁的扭矩、效率、铁损(贝尔托蒂)和稳态速度时间分别为37.52牛米、91.1%、84.78瓦和0.25秒，与其他材料的性能。进一步测试了这些材料在两种情况下（无负载和负载）的性能。

关键词： 磁芯材料、电机性能、感应电机、磁通环境、有限元。

1. Introduction

The squirrel cage three-phase squirrel cage induction motor (SCIM) is generally used in our households and industries because it is cheapest, easy to repair, and consistent. On the other hand, electric motors account for around 30% to 80% of total electricity consumption in the internal industrial sector [1]. More than 50% of electrical energy generated being utilized by Induction motors accounted for almost 60% of all industrial electricity consumption [2]. These motors are notably appropriate for applications that should keep the motor at a constant speed, be self-starting, or require low

Received: May 25, 2021 / Revised: June 6, 2021 / Accepted: July 22, 2021 / Published: August 30, 2021

About the authors: Ali Failh Challoop, Ahmed Jasim Sultan, Electrical Power Engineering Department, Electrical Engineering Technical College, Middle Technical University, Baghdad, Iraq; Mehdi F. Bonneya, Kut Technical Institute, Middle Technical University, Wasit, Iraq

maintenance. This motor is typically the natural choice as a drive in industry due to its simplicity, robustness, relatively low cost, and low maintenance. When a fairly constant speed of operation is required, the squirrel cage motor is frequently chosen [3]. Therefore, Manufacturers must develop ranges of highly efficient motors that require careful design of motor. The dependence on new materials and technologies is inventive. Due to their prevalence, magnetic materials play an important role in improving the performance of motors [4]. Concerning this aim, its major advantages are the permeability of magnetic material and the losses of specific. New, advanced types of motors that have high efficiency, choosing a magnetic substance is today's “open trouble.” (If the major issue is not the entire cost), it is known that copper merge for induction motor squirrel cage rotor bars and end rings instead of aluminum will result in Improvement's fascinating in the efficiency of the motor. It is noted through the induction motor designing, Mechanical properties of the motor, such as the electromagnetic torque, will it improve or not, and we will notice this through the results obtained. Modeling of electromagnetic analysis of induction motor can be performed in any commercial packages programming like Altair flux, COMSOL Multiphysics and ANSYS SOFTWARE. All these programming software depend on finite element analysis (FEA). In [5], this paper was presented by obtaining the effect of several magnetic materials during the design stage of the three-phase squirrel cage induction motor that saves energy (which both the stator and the rotor are reliant on) on several quantities, including weight, cost, efficiency, power factor, and developed output torque. This research aims to describe the major aspects of examining the effect on motor performance to improve or weaken three-phase induction motors. When a greater number of electric steels are used in the stator or rotor core, this work focused on selecting several ideal alloys for a squirrel cage three-phase induction motor. Concerns are focused on studying future motor design, as well as studying the greater impact of modern materials and their impact on applicability and performance. In [6], suggested a simulation of the dynamic start-up behavior of an induction motor with a direct link via the Internet to the network was performed using the COMSOL program, and the motor's selected electrical and mechanical parameters were investigated, and the results were given. The finite element approach is used to analyze the electromagnetic field and discover answers to engineering problems, and this program is based on it. The goal of this project is to simulate the major motor characteristics during machine start-up under various conditions and to compare the selected parameters, such as speed, currents, and torque, with experimentally measured values. The results showed that the parameters of the chosen simulated motor matched the measurement parameters. The currents in the rotor bar also have a significant impact on the torque and speed cycles. [7] suggested a simulation of squirrel cage induction motor using COMSOL multiphysics software for the given motor operating circumstances. The purpose of this work is to compare simulated motor parameters to motor catalog parameters and real measurements, as well as theoretical presumptions, the simulation findings of the induction motor model, notably for the nominal operating condition, closely match the motor catalog values and the measured values. The stator current values simulated and measured varied just slightly. [8] presented a model of a squirrel cage three-phase induction motor using a COMSOL environment to decrease the three-dimension model. The interaction of physic interfaces, such as electrical circuits and rotating machinery, was studied using a quasi-3D model. This study depends on time. An induction motor is a sophisticated electromagnetic device featuring numerous phenomena, including a magnetic field, electrical circuits, and mechanical rotation. It's critical to develop their models to aid in a better understanding of these events. In [9], the authors proposed shortening the duration of the IM's numerical transient in time-stepping FEA so that the steady-state can be reached quickly. By removing or lowering the stator and rotor electromagnetic time constants independently, the suggested approach is capable of establishing a starting condition for the simulation that is near the final steady state. The proposed simulation method reduces the initial simulation time by 34% (solid-rotor IM) and 70% (squirrel cage IM). As a result, the suggested approach is more efficient for solid-rotor IMs with a long rotor electromagnetic time constant. This study aims to use five materials in the case study induction motor by using Altair flux programs to obtain good performance for the motor.

2. Hypothesis of This Article

(A) Modelling and analysis of induction motor parameters and behavior (torque, efficiency, iron losses, etc.) under no-load and load conditions;

(B) Choosing core magnetic materials;

(C) Distribution of flux density;

(D) Visualizing current density in the rotor bar of the rotor;

(E) The results show that Nickel-Iron gives a good performance of induction motor.

3. Modeling of an Induction Motor in Three Phases

Two magnetic fields are present in the induction motor, the first of which is activated by currents in the three-phase stator circuit and the second of which is excited by currents in the rotor circuit. The machine has an electromagnetic coupling between them. The inner torque of the motor is produced as a result of their interaction [10]. Motor modeling requires careful planning of the motor's geometry. The properties of the precise magnetic materials and the electrical circuit components represent the effects of the overhang and the appropriate design of the network, especially the air gap.

The electromagnetic field in an induction motor is given by the following Maxwell's equations [11, 12]:

$$\nabla . B = 0 \quad (1)$$

where:

B - Magnetic flux density (tesla).

$$\nabla \times E = \frac{-\partial B}{\partial t} \quad (2)$$

where:

E - electric field intensity (V/m).

$$\nabla \times H = J + \frac{\partial D}{\partial t} \quad (3)$$

where:

H - magnetic field intensity (A/m);

$J -$ Electric current density (A/m^2);

D - electric flux density/displacement field in (As/m^2).

The following equations are used to model a time-dependent investigation of the magnetic field in motor parts as:

$$\sigma \frac{\partial A}{\partial t} + \nabla \times H - \sigma v \times B = J_e \quad (4)$$

where:

σ - the conductivity of electricity in (S·m^{-1});

A - the potential of the magnetic vector in (V·s·m^{-1});

v: is the velocity of conductors in (m·s^{-1});

$J_e -$ the current density produced externally in (A·m^{-2}).

In the model of an induction motor with a multi-turn coil, the externally generated current density (J_e) for the stator slot is formulated as:

$$J_e = \frac{NI}{A}\,\mathrm{e} \quad (5)$$

where:

N - the number of turns of the stator coil;

A - the total cross-section area of the coil domain;

$I -$ the phase current of the stator;

e - The direction of the wires in the slot is represented by the vector field (e).

Single-turn coil domains are used to form the rotor slots, and the externally generated current density for the time-dependent investigation is defined as:

$$J_e = \sigma \frac{V}{d}\,\mathrm{e} \quad (6)$$

where:

V - the electrical potential applied to the rotor bar in the case of a coil turn (V);

d - the thickness of out-of-plane physics in (m).

One of the most popular and common methods used for calculating the core loss in this type of induction motor is the Steinmetz equation, which depends on the highest magnetic flux density and the frequency of magnetization [13].

Steinmetz equation is

$$P_c = K\, f^{\alpha} B_m^{\beta} \quad (7)$$

where k, α, and β are known as Steinmetz parameters.

Bertotti successfully developed the Steins equation for magnetization, which can calculate complex hysteresis phenomena [14]. The energy loss in magnetic materials that are subject to an alternating magnetic field at low and medium frequencies is a result of eddy currents in the magnetic material, which is characterized by its specific conductivity [15]. The common empirical model for calculating the core loss is under the source of the sinusoidal excitation, which is the Bertotti loss separation theory, which is a well-established model for predicting the core losses based on the separation of iron losses in formula P_{Fe} into three factors: losses due to static hysteresis P_{hyst}, Eddy current losses in a dynamic environment P_{ec}, and the excess losses P_{exc}. An additional loss term P_{exc} is to take into account the excess losses in relation to frequency and flux density [16, 17].

Bertotti loss equation is given by

$$P_{Fe} = P_{hyst} + P_{ec} + P_{exc} = K_h f^{\alpha} B_m^{\beta} + K_e f^2 B^2 + C_{exc} f^{1.5} B^{1.5} \quad (8)$$

where:

$K_h -$ coefficient of hysteresis loss;

$K_e -$ the coefficient of eddy current loss;

B_m - the peak flux density.

$$C_{exc} = \sqrt{S V_o \sigma G}.$$

where:

S - the lamination sample's cross-sectional area;

G - a dimensionless eddy current damping coefficient ≈ 0.136;

$\sigma -$ the lamination's electrical conductivity;

$V_o -$ characterizes the distribution of statistical of the local coercive fields.

4. 2D-FEM of SCIM

The SCIM 2D is modeled in the flux environment, which is dependent on FEM. It is used to model electrical machinery, analyze magnetic fields and calculate the behavior of electric devices. This procedure is used before an electrical machine is manufactured and pre-tested. Thus, the induction motor makes use of the material's properties as well as the motor's physical dimensions. In both the no-load and load cases, we may compute flux distributions and generated torque [6, 7].

5. Numerical Results

The system parameters of SCIM, as tabulated in Table 1, were used by using the Flux environment to design a squirrel cage three-phase induction motor with a cross section, as shown in Fig. 1. The induction motor was constructed based on the major geometric parameters shown in the table. The data of this motor were entered into the program, and the proposed motor was designed through simulation of this program based on FEM analysis. The slots of the stator and the rotor bars of the rotor were also designed according to the dimensions of the motor. More than one magnetic material was selected for the core of the stator and rotor and changed to obtain the induction motor's best performance.

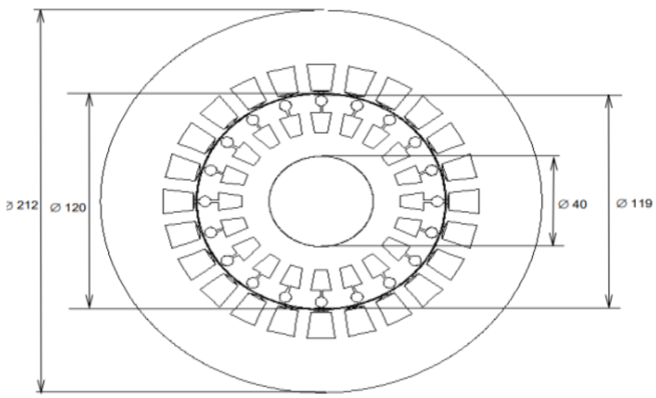

(a)

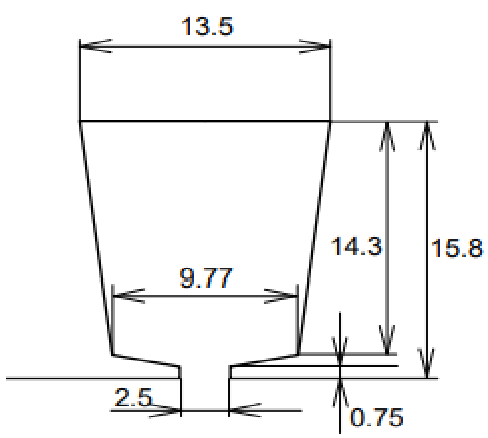

(b)

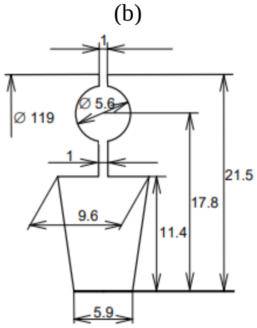

(c)

Fig. 1 a) Cross-section of the stator and rotor armatures, b) stator slot dimensions, c) rotor slot dimensions

Table 1 The parameters of the motor

Parameters	Values
The number of stator slots	24
The number of rotor bars.	20
Nominal voltage	380 V
Nominal current	8.4 A
Nominal frequency	50 [Hz]
The outer diameter of the stator	212 mm
The outer diameter of the rotor	119 mm
The rotor shaft radius	20 mm
Nominal speed	2998 rpm
Nominal power factor	0.85
The thickness of the air gap	0.5 mm
The diameter of the rotor shaft	52 mm
Stator tooth width	2.5 mm

Fig. 2a shows the induction machine model that resulted. The field lines and flux density levels for the high power working zone are also depicted. As indicated in Fig. 2b, the FE model is used with the machine equivalent electrical diagram. The (FE) also represents the stator windings and the squirrel cage by using coil conductors (2) or a squirrel cage component (4) as field-circuit coupling elements. This electrical diagram allows you to define all of the external electrical elements that need to be taken into account, such as power sources and stator winding end turn impedances.

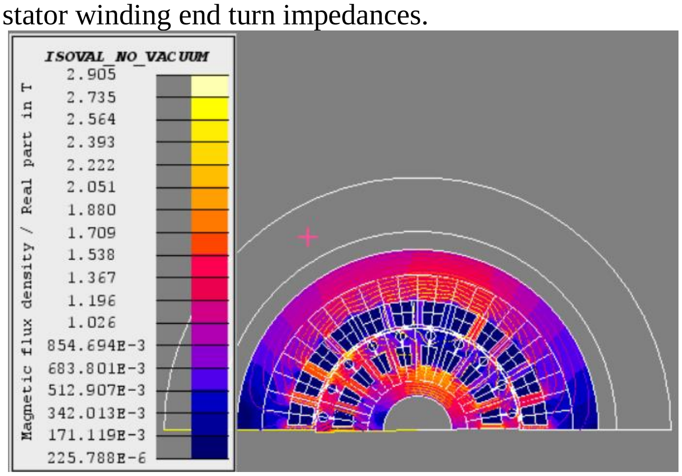

(a)

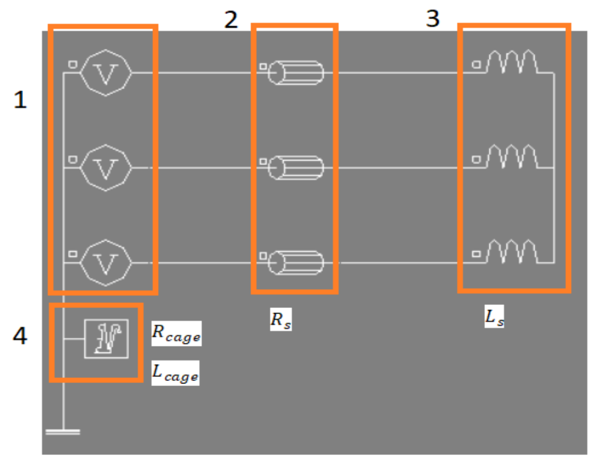

(b)

Fig. 2 a) At higher power operating point, studied machine 2D FE model with flux density levels and field lines (the flux density range is limited to 2.9T, and the saturated portions are shown in yellow), b) 2D FE model of the analyzed machine's electrical diagram with (1) sources of voltage, (2) Components for field-circuit coupling, (3) stator end winding inductance and (4) squirrel cage

The yellow color in Fig. 3 indicates the high distribution of magnetic flux density in the rotor area that the induction motor gets in the case of overload or high temperature. This state changes from one material to another. Also, the max current density is about 5.225e6 (A/m^2) on rotor bars, and these values will change from one magnetic material to another, as shown in Fig. 4.

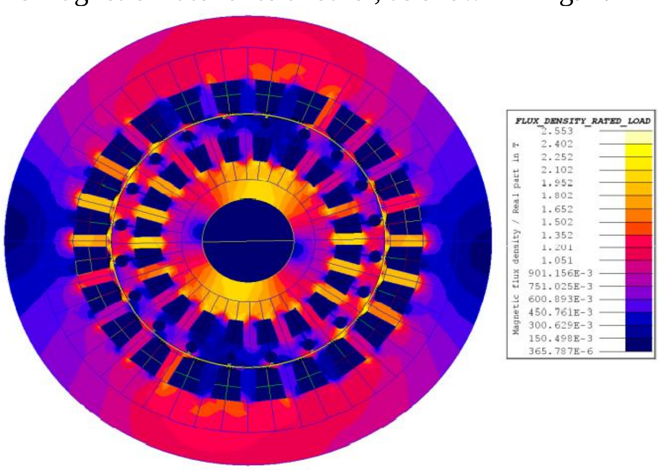

Fig. 3 Distribution of magnetic flux density

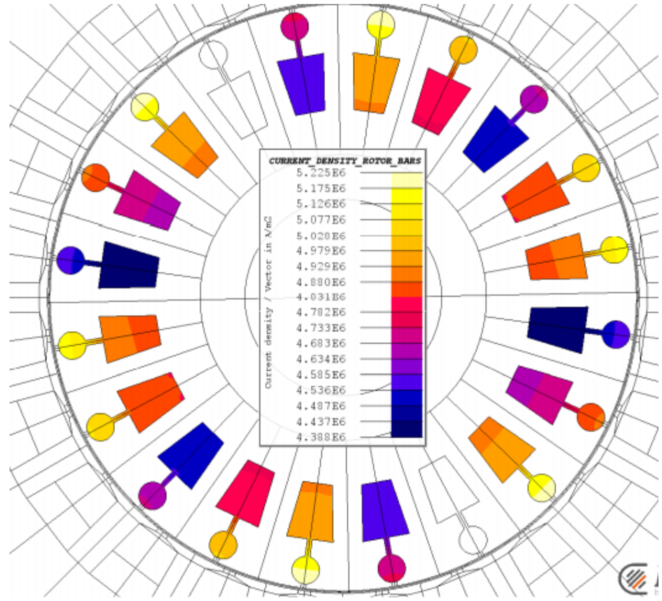

Fig. 4 Current density in the rotor bars

It has been observed through Fig. 5 and 6 that according to the use of a variety of magnetic materials for the stator and rotor core. It is the NICKEL IRON material that gives the best stability for the speed and the least time in terms of reaching the steady-state time that it can be ($t_{ss} = 0.25\, sec$) as shown below and also it gives minimum average cogging torque as mentioned below and is considered the good material in terms of cost and performance of the induction motor compared to other materials.

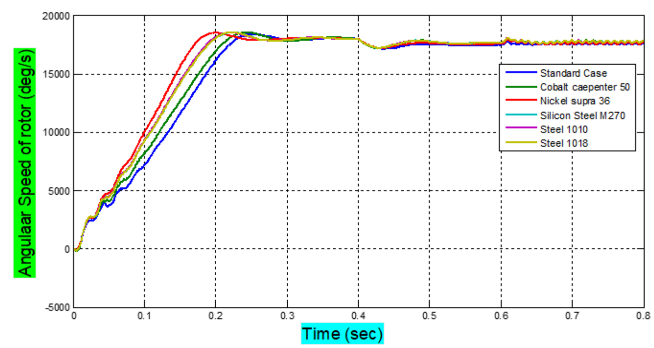

Fig. 5 Angular speed of the motor with respect to the time

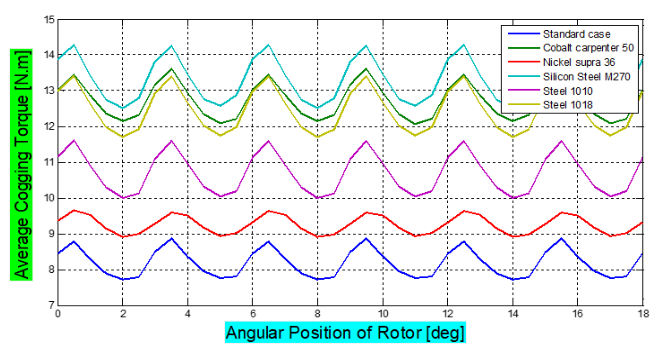

Fig. 6 Average cogging Torque against Angular position of the rotor

As can be seen from the results of the waveforms, the motor starts with a load equal to the nominal torque. The start of operation is associated with high currents of up to (90 A) as shown in Fig. 7 and also high oscillations in the internal torque of the motor that corresponds to the motor speed as shown in Fig. 9. In 0.3 sec, the machine reaches a stable state with speed equal to (2904 rpm). Fig. 10 shows the geometry of the induction motor through the magnetic flux density and isolines of the magnetic vector potential.

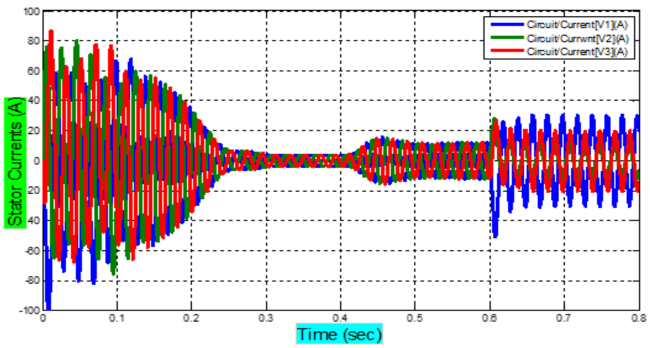

Fig. 7 Waveform of staring stator current

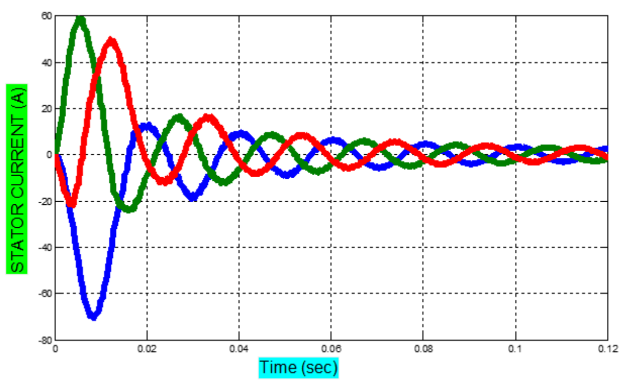

Fig. 8 Waveform of stator current with respect to time

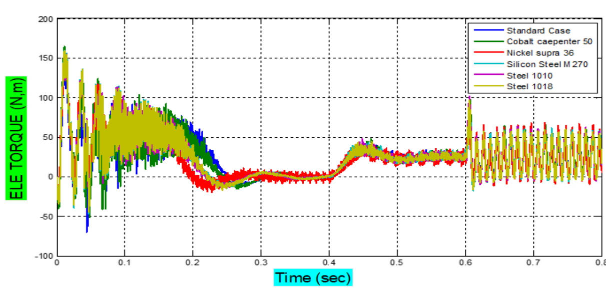

Fig. 9 Electromagnetic torque with respect to time

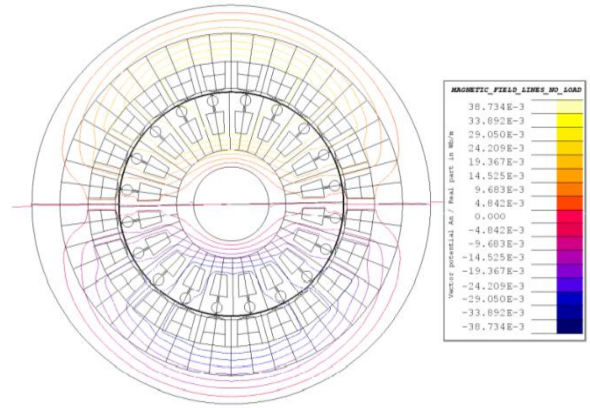

(a)

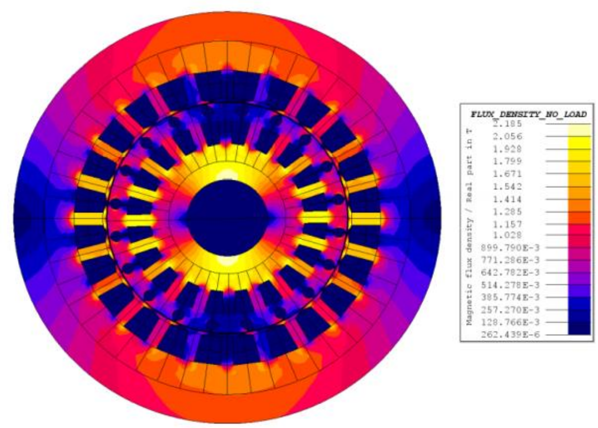

(b)

Fig. 10 a) The isolines of the magnetic vector potential (An) in (wb/m^2), b) the isovalues of the magnetic flux density in (T)

The goal is to analyze the transient behavior of the motor for rated speed considering the magnetic field harmonics caused by stator slotting, rotor, and the rotor motion, based on transient magnetic simulations with a rated rotor speed constant. We calculate the motor torque values taking into account magnetic field harmonics caused by armature slotting and rotor rotation. Different materials were used for each simulation. The different losses in stator and rotor, the output power, torque, and efficiency are computed, and the results are compared to standard case material.

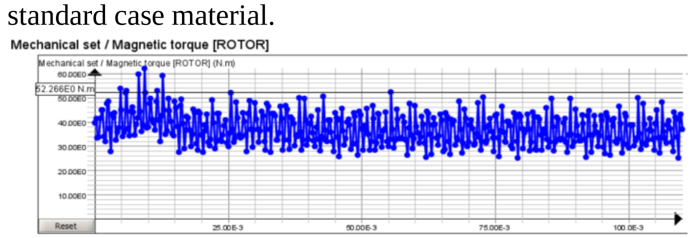

Time (sec)

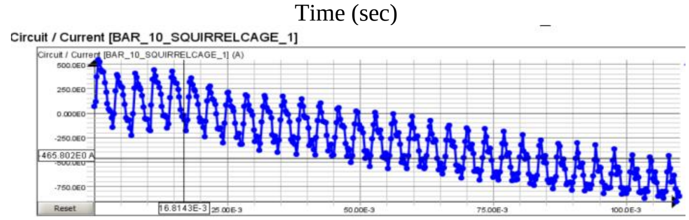

Time (sec)

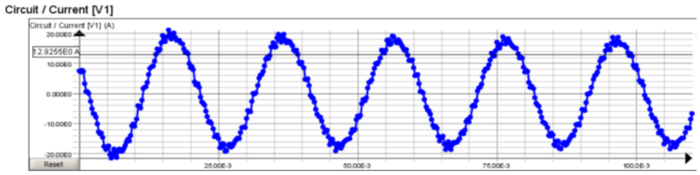

Time (sec)

Fig. 11 Waveform of torque, bar current, and stator current in transient behavior case of the motor

Table 2 Standard case STEEL _NLIN material of stator part and rotor

Values	**Case (N.L) S = 0.001**	**Case (F.L) S = 0.001**
Stator Current (I_rms) = (I_STA) (A)	3.33	8.35
Stator Losses (PJS) (W)	51.37	322.6
Rotor Losses (PJR) (W)	0.26	247.06
Iron Losses (2*bertotti) (W)	27.66	27.79
Power transmitted to the rotor (PTR) = (P_g) (W)	260.926	7720.65
Shaft Power (output mechanical power) = (PU) (W)	260.665	7473.597
Absorbed Power (PA) (W)	312.3	8043.339
Electrical Input Power (w)	___	8041.4
Torque (N.m)	0.82	23.78
Efficiency %	76.67 %	92.59 %
Steady State time of Speed (t_{ss}) (sec)	____	0.314
Magnetic flux density [B_{max}] [T]	2.181	2.561
Max current density (A/m^2)	163.482E3	5.225e6
Cogging Average Torque [T_g][N.m]	8.28608	_______

Table 3 Core materials of performance of induction motor at no load (N.L)

Test Case	**Case (N.L) S=0.001**				
Core Materials	**Cobalt Iron (carpenter 50 DC)**	**Steel_ 1010 _XC10)**	**Steel 1018**	**Silicon Steel M270**	**Nickel Iron (Supra 36)**
Stator Current (I_rms) = (I_STA) (A)	2.25	6.14	6.16	4.03	14.04
Stator Losses (PJS) (W)	23.51	174.41	175.56	75.33	911.47
Rotor Losses (PJR) (W)	0.41	0.34	0.4	0.43	0.29
Iron Losses (2 * Bertotti) (W)	94.53	92.64	92.4	95.86	88.52
Power transmitted to the rotor (PTR)= (P_g) (W)	411.939	341.86	400.56	429.07	295.2
Shaft Power (output mechanical power= (PU) (W)	411.527	341.52	400.15	428.64	294.91
Absorbed Power (PA) (W)	435.4525	516.28	576.12	504.4	1206.68
Torque (N.m)	1.3	1.08	1.27	1.36	0.938
Efficiency %	77.64	56.06	59.8	71.4	22.76
Cogging Average Torque [T_g][N.m]	12.84595	10.800325	12.5498	12.60075	9.276295
Magnetic flux density [B_{max}] [T]	2.211	2.003	2.069	2.121	2.017
Max current density (A/m^2)	246.153E3	245.636E3	292.665E3	290.341E3	308.008E3

Table 4 Core materials of behavior of machine at full load (F.L)

Test Case	**Case (F.L) S = 0.032**				
Core Materials	**Cobalt Iron (carpenter 50 DC)**	**Steel_ 1010 _XC10)**	**Steel 1018**	**Silicon Steel M270**	**Nickel Iron (Supra 36)**
Stator Current (I_rms) = (I_STA) (A)	11.54	12.09	13.57	13	16.35
Stator Losses (PJS) (W)	615.8	676.06	851.6	786.35	1235.97
Rotor Losses (PJR) (W)	355.96	322.11	362.26	377.65	285.82
Iron Losses (2*bertotti) (W)	89.96	86.96	85.82	89.63	84.78
Power transmitted to the rotor (PTR) = (P_g) (W)	11123.76	10065.94	11320.67	11801.72	8928.3
Shaft Power (output mechanical power= (PU) (W)	10767.8	9743.83	10958.41	11424.07	9342.59
Absorbed Power (PA) (W)	11739.59	10742	12172.28	12588.07	10168.16
Electrical Input Power (w)	11734.4121	10735.95	12166.2	12591.163	10164.27
Torque (N.m)	34.27	31.01	34.88	36.35	37.52
Efficiency %	90.02	89.9	89.41	90.1	91.1
Steady State time of Speed (t_{ss}) (sec)	0.35	0.318	0.32	0.311	0.25
Bar Current [A]	487.505	254.918	528.792	407.972	468.463
Magnetic flux density [B_{max}] [T]	2.583	2.280	2.409	2.905	2.244

Max current density (A/m²)	8.130E6	7.892E6	9.531E6	9.622E6	9.755E6

6. Conclusion

Magnetic materials are crucial in constructing electrical machines, particularly induction motors, which require only soft magnetic materials (no permanent magnets). So the engineer's design must select a lot of the optimal and commercially available alloys such as iron, nickel, and cobalt. To achieve the design's magnetic qualities, the engineer must make several trade-offs on many magnetic materials about the electrical, mechanical, and physical properties of the materials. The present work emphasized the procedure for selecting the optimum alloys for a squirrel cage three-phase induction motor better than redesigning the device. For the best performance of the induction motor, many magnetic materials of the stator and rotor cores have been changed and study their effects on different quantities such as efficiency, torque, rotor speed, and other quantities. Therefore, the results indicated that Nickel iron material is the best in terms of performance and price and gives good behavior to the motor compared to other materials.

References

[1] NUGROHO H. S., MAHARDHIKO S. W., and HARYOSENO H. W. Life cycle cost assessment of replacing standard induction motor with high efficiency induction motor used in salt industry. *AIP Conference Proceedings*, 2019, 2062: 020033. https://doi.org/10.1063/1.5086580

[2] GANGSAR P., & TIWARI R. Diagnostics of mechanical and electrical faults in induction motors using wavelet-based features of vibration and current through support vector machine algorithms for various operating conditions. *Journal of the Brazilian Society of Mechanical Sciences and Engineering*, 2019, 41(2): 71. https://doi.org/10.1007/s40430-019-1574-5

[3] BIRD J. *Electrical Circuit Theory and Technology*, 6th ed. Routledge, 2017.

[4] MATIZAMHUKA W. The impact of magnetic materials in renewable energy-related technologies in the 21st century industrial revolution: The case of South Africa. *Advances in Materials Science and Engineering*, 2018, 2018: 3149412. https://doi.org/10.1155/2018/3149412

[5] KARNAVAS Y. L., & CHASIOTIS I. D. Influence of soft magnetic materials application to squirrel cage induction motor design and performance. *Engineering Journal*, 2017, 21(1): 193–206. https://doi.org/10.4186/ej.2017.21.1.193

[6] KOCMAN S., ORSAG P., and PECINKA P. Simulation of start-up behaviour of induction motor with direct online connection. *Advances in Electrical and Electronic Engineering*, 2017, 15(5): 754–762. https://doi.org/10.15598/aeee.v15i5.2342

[7] KOCMAN S., ORSAG P., and PECINKA P. Simulation of selected induction motor operating conditions using COMSOL software. *Advances in Electrical and Electronic Engineering*, 2018, 16(3): 288–296. https://doi.org/10.15598/aeee.v16i3.2824

[8] KOCMAN S., PE P., and HRUBÝ T. Induction Motor Modeling Using COMSOL Multiphysics. Proceedings of the 17th International Scientific Conference on Electric Power Engineering, Prague, 2016, pp. 1-5. https://doi.org/10.1109/EPE.2016.7521727

[9] DI C., PETROV I., PYRHONEN J. J., and CHEN J. Accelerating the Time-Stepping Finite-Element Analysis of Induction Machines in Transient-Magnetic Solutions. *IEEE Access*, 2019, 7: 122251–122260. https://doi.org/10.1109/ACCESS.2019.2938269

[10] KOCMAN S., & NOWAK S. Analysis of the stator winding fault of induction motor using COMSOL multiphysics. Proceedings of the 20th International Scientific Conference on Electric Power Engineering, Kouty nad Desnou, 2019, pp. 1–6. https://doi.org/10.1109/EPE.2019.8778128

[11] BOLOTIN K., SHVYDKIY E., SMOLYANOV I., and TARASOV F. Numerical study of the possibility of using cermet inserts in electromagnetic stirring application. *Acta Technica CSAV (Ceskoslovensk Akademie Ved)*, 2018, 63(5): 709–720. http://journal.it.cas.cz/63(2018)-5/Complete%20Issue%2063(2018)-5.pdf

[12] YETGIN A. G., & UNLUKAYA E. New design in order to reduce rotor reaction for squirrel cage induction motor: Skewed slits. *Journal of Electrical Systems*, 2018, 14(1): 1–12. https://www.journal.esrgroups.org/jes/papers/14_1_1.pdf

[13] BARG S., AMMOUS K., MEJBRI H., and AMMOUS A. An Improved Empirical Formulation for Magnetic Core Losses Estimation Under Nonsinusoidal Induction. *IEEE Transactions on Power Electronics*, 2017, 32(3): 2146–2154. https://doi.org/10.1109/TPEL.2016.2555359

[14] YANLI F., & CHENGNING Z. Analytical Calculation for Predicting the Core Loss of Surface-Mounted Permanent Magnet Machine. *Energy Procedia*, 2017, 105: 2119–2124. https://doi.org/10.1016/j.egypro.2017.03.595

[15] AHMADI F., SOZER Y., DONAHUE M. J., and TSUKERMAN I. A Low-loss and Lightweight Magnetic Material for Electrical Machinery. *IET Electric Power Applications*, 2020, 14(2): 282-290. https://doi.org/10.1049/iet-epa.2019.0430

[16] RAZZAQ M. K. *Loss Identification Using Inverse Thermal Modelling in Cage Induction Motor*. Master thesis. Aalto University, Espoo, 2019. https://aaltodoc.aalto.fi/bitstream/handle/123456789/37922/master_Razzaq_Muhammad_2019.pdf?sequence=1

[17] ZHAO Z., HU X., BI Z., XU M., MA X., and ZHANG P. Calculation of core loss under distorted flux density with minor hysteresis loops for laminated steel structure. *AIP Advances*, 2020, 10(7): 075001. https://doi.org/10.1063/5.0005248

参考文:

[1] NUGROHO H. S.、MAHARDHIKO S. W. 和 HARYOSENO H. W. 用盐业中使用的高效感应电机替换标准感应电机的生命周期成本评估。AIP会议论文集，2019，2062：020033。https://doi.org/10.1063/1.5086580

[2] GANGSAR P., & TIWARI R. 使用基于小波的振动和电流特征通过支持向量机算法在各种操作条件下诊断感应电机中的机械和电气故障。巴西机械科学与工程学会杂志，2019，41(2): 71. https://doi.org/10.1007/s40430-019-1574-5

[3] BIRD J. 电路理论与技术，第 6 版。劳特利奇，2017。

[4] MATIZAMHUKA W. 磁性材料对21世纪工业革命中可再生能源相关技术的影响：以南非为例。材料科学与工程进展, 2018, 2018: 3149412. https://doi.org/10.1155/2018/3149412

[5] KARNAVAS Y. L., & CHASIOTIS I. D. 软磁材料应用对鼠笼式感应电机设计和性能的影响。工程杂志, 2017, 21(1): 193–206。https://doi.org/10.4186/ej.2017.21.1.193

[6] KOCMAN S.、ORSAG P. 和 PECINKA P. 直接在线连接感应电机启动行为的仿真。电气与电子工程进展, 2017, 15(5): 754–762。https://doi.org/10.15598/aeee.v15i5.2342

[7] KOCMAN S.、ORSAG P. 和 PECINKA P. 使用COMSOL软件模拟选定的感应电机运行条件。电气与电子工程进展, 2018, 16(3): 288–296。https://doi.org/10.15598/aeee.v16i3.2824

[8] KOCMAN S.、PE P. 和 HRUBÝ T. 使用COMSOL多物理场进行感应电机建模。第17届国际电力工程科学会议论文集，布拉格，2016，第 1-5 页。https://doi.org/10.1109/EPE.2016.7521727

[9] DI C.、PETROV I.、PYRHONEN J. J. 和 CHEN J. 加速瞬态磁解决方案中感应电机的时间步进有限元分析。IEEE访问，2019，7：122251–122260。https://doi.org/10.1109/ACCESS.2019.2938269

[10] KOCMAN S., & NOWAK S. 使用COMSOL多物理场分析感应电机定子绕组故障。第20届国际电力工程科学会议论文集，考蒂纳德斯努，2019，第 1-6 页。 https://doi.org/10.1109/EPE.2019.8778128

[11] BOLOTIN K.、SHVYDKIY E.、SMOLYANOV I. 和 TARASOV F. 在电磁搅拌应用中使用金属陶瓷插件的可能性的数值研究。技术学报（捷克斯洛伐克科学院），2018，63(5): 709–720。http://journal.it.cas.cz/63(2018)-5/Complete%20Issue%2063(2018)-5.pdf

[12] YETGIN A. G., & UNLUKAYA E. 为减少鼠笼式感应电机转子反作用而设计的新设计：斜缝。电气系统杂志, 2018, 14(1): 1-12。https://www.journal.esrgroups.org/jes/papers/14_1_1.pdf

[13] BARG S.、AMMOUS K.、MEJBRI H. 和 AMMOUS A. 非正弦感应下磁芯损耗估计的改进经验公式。IEEE电力电子学报，2017，32(3)：2146–2154。https://doi.org/10.1109/TPEL.2016.2555359

[14] YANLI F., & CHENGNING Z. 预测表面贴装永磁电机磁芯损耗的分析计算。能源学报，2017，105：2119-2124。https://doi.org/10.1016/j.egypro.2017.03.595

[15] AHMADI F.、SOZER Y.、DONAHUE M. J. 和 TSUKERMAN I. 一种用于电机的低损耗轻质磁性材料。国际教育与培训中心电力应用，2020，14(2)：282-290。https://doi.org/10.1049/iet-epa.2019.0430

[16] RAZZAQ M. K. 在笼式感应电机中使用逆热模型进行损耗识别。硕士论文。阿尔托大学，埃斯波，2019。https://aaltodoc.aalto.fi/bitstream/handle/123456789/37922/master_Razzaq_Muhammad_2019.pdf?sequence=1

[17] ZHAO Z., HU X., BI Z., XU M., MA X., 和 ZHANG P. 计算具有较小磁滞回线的叠层钢结构畸变磁通密度下的磁芯损耗。AIP 预付款, 2020, 10(7): 075001. https://doi.org/10.1063/5.0005248